

# Visual descriptors for content-based retrieval of remote sensing images

Paolo Napoletano

Received: date / Accepted: date

**Abstract** In this paper we present an extensive evaluation of visual descriptors for the content-based retrieval of remote sensing (RS) images. The evaluation includes global, local, and Convolutional Neural Network (CNNs) features coupled with four different Content-Based Image Retrieval schemes. We conducted all the experiments on two publicly available datasets: the 21-class UC Merced Land Use/Land Cover (LandUse) dataset and 19-class High-resolution Satellite Scene dataset (SceneSat). The content of RS images might be quite heterogeneous, ranging from images containing fine grained textures, to coarse grained ones or to images containing objects. It is therefore not obvious in this domain, which descriptor should be employed to describe images having such a variability. Results demonstrate that CNN-based and local features are the best performing whatever is the retrieval scheme adopted. In particular, CNN-based descriptors are more effective than local descriptors in the case of the LandUse dataset and less effective than local-based descriptors in the case of the SceneSat dataset.

**Keywords** Content-Based Image Retrieval (CBIR) · Visual Descriptors · Convolutional Neural Networks (CNNs) · Relevance Feedback (RF) · Active Learning (AL) · Remote Sensing (RS).

## 1 Introduction

The recent availability of a large amount of remote sensing (RS) images is boosting the design of systems for

their management. A conventional RS image management system usually exploits *high-level* features to index the images such as textual annotations and metadata [18]. In the recent years, researchers are focusing their attention on systems that exploit *low-level* features extracted from images for their automatic indexing and retrieval [28]. These types of systems are known as Content-Based Image Retrieval (CBIR) systems and they have demonstrated to be very useful in the RS domain [19, 1, 44, 63, 64].

The CBIR systems allow to search and retrieve images that are similar to a given query image [55, 18]. Usually their performance strongly depends on the effectiveness of the features exploited for representing the visual content of the images [55]. The content of RS images might be quite heterogeneous, ranging from images containing fine grained textures, to coarse grained ones or to images containing objects [62, 17]. It is therefore not obvious in this domain, which descriptor should be employed to describe images having such a variability.

In this paper we compare several visual descriptors in combination with four different retrieval schemes. Such descriptors can be grouped in three classes. The first class includes traditional global descriptors that were originally designed for image analysis. The second one includes local features that were originally designed for object recognition. The third class includes features that correspond to intermediate representations of Convolutional Neural Networks (CNNs) trained for generic object and/or scene recognition.

To reduce the influence of the retrieval scheme on the evaluation of the features we investigated the features coupled with four different image retrieval schemes. The first one, that is also the simplest one, is a *basic* image retrieval system that takes one image as input query and returns a list of images ordered by their de-

DISCo, Department of Informatics, Systems and Communication, University of Milano-Bicocca  
Viale Sarca 336, Milan 20126, Italy  
E-mail: {paolol.napoletano}@unimib.it

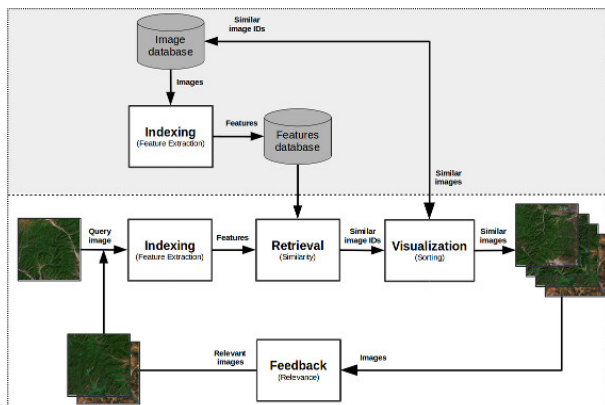


Fig. 1 Main components of a CBIR system.

gree of feature similarity. The second and the third ones, named *pseudo* and *manual Relevance Feedback* (RF), extend the *basic* approach by expanding the initial query. The *Pseudo RF* scheme uses the  $n$  most similar images to the initial query, for re-querying the image database. The final result is obtained by combining the results of each single query. In the *manual RF*, the set of relevant images is suggested by the user which evaluates the result of the initial query. The last scheme considered is named *active-learning-based RF* [19]. It exploits Support Vector Machines (SVM) to classify relevant and not relevant images on the basis of the user feedback.

For the sake of completeness, for the first three retrieval schemes we considered different measure of similarity, such as Euclidean, Cosine, Manhattan, and  $\chi^2$ -square, while for the *active-learning-based RF* scheme we considered the histogram intersection as similarity measure, as proposed by the original authors [19].

We conducted all the experiments on two publicly available datasets: the 21-class UC Merced Land Use/Land Cover dataset [62] (LandUse) and 19-class High-resolution Satellite Scene dataset [17] (SatScene). Evaluations exploit several computational measures in order to quantify the effectiveness of the features. To make the experiments replicable, we made publicly available all the visual descriptors calculated as well as the scripts for making the evaluation of all the image retrieval schemes<sup>1</sup>.

The rest of the paper is organized as follows: Section 2 reviews the most relevant visual descriptors and retrieval schemes; Section 3 describes the data, visual descriptors, retrieval schemes evaluated and the experimental setup; Section 4 reports and analyzes the experimental results; finally, Section 5 presents our final considerations and discusses some new directions for our future research.

## 2 Background and Related Works

A typical Content-Based Image Retrieval (CBIR) system is composed of four main parts [55,18], see Fig. 1:

1. The *Indexing*, also called *feature extraction*, module computes the visual descriptors that characterize the image content. Given an image, these features are usually pre-computed and stored in a *database of features*;
2. The *Retrieval* module, given a query image, finds the images in the database that are most similar by comparing the corresponding visual descriptors.
3. The *Visualization* module shows the images that are most similar to a given query image ordered by the degree of similarity.
4. The *Relevance Feedback* module makes it possible to select relevant images from the subset of images returned after an initial query. This selection can be given manually by a user or automatically by the system.

### 2.1 Indexing

A huge variety of features have been proposed in literature for describing the visual content. They are often divided into *global* and *local*.

Global features describe an image as a whole in terms of color, texture and shape distributions [40]. Some notable examples of global features are color histograms [41], spatial histogram [60], Gabor filters [36], co-occurrence matrices [2,25], Local Binary Patterns (LBP) [42], Color and Edge Directivity Descriptor (CEDD) [11], Histogram of Oriented Gradients (HOG) [30], morphological operators like granulometries information [1,24], Dual Tree Complex Wavelet Transform (DT-CWT) [7, 4] and GIST [43]. Readers who would wish to deepen the subject can refer to the following papers [49,21,33, 59].

*Local* descriptors like Scale Invariant Feature Transform (SIFT) [34,5] provide a way to describe salient patches around properly chosen key points within the images. The dimension of the feature vector depends on the number of chosen key points in the image. A great number of key points can generate large feature vectors that can be difficult to be handled in the case of a large-scale image retrieval system. The most common approach to reduce the size of feature vectors is the *Bag-of-Visual Words* (BoVW) [54,62]. This approach has shown excellent performance not only in image retrieval applications [21] but also in object recognition [23], image classification [15] and annotation [57]. The idea underlying is to quantize by clustering local descriptors

<sup>1</sup> <http://www.ivl.disco.unimib.it/activities/cbir-rs/>

into *visual words*. Words are then defined as the centers of the learned clusters and are representative of several similar local regions. Given an image, for each key point the corresponding local descriptor is mapped to the most similar visual word. The final feature vector of the image is represented by the histogram of the its visual words.

Convolutional Neural Networks (CNNs) are a class of learnable architectures used in many domains such as image recognition, image annotation, image retrieval etc [51]. CNNs are usually composed of several layers of processing, each involving linear as well as non-linear operators, that are learned jointly, in an end-to-end manner, to solve a particular tasks. A typical CNN architecture for image classification consists of one or more convolutional layers followed by one or more fully connected layers. The result of the last full connected layer is the CNN output. The number of output nodes is equal to the number of image classes [31].

A CNN that has been trained for solving a given task can be also adapted to solve a different task. In practice, very few people train an entire CNN from scratch, because it is relatively rare to have a dataset of sufficient size. Instead, it is common to take a CNN that is pre-trained on a very large dataset (e.g. ImageNet, which contains 1.2 million images with 1000 categories [20]), and then use it either as an initialization or as a fixed feature extractor for the task of interest [47,58]. In the latter case, given an input image, the pre-trained CNN performs all the multilayered operations and the corresponding feature vector is the output of one of the fully connected layers [58]. This use of CNNs have demonstrated to be very effective in many pattern recognition applications [47].

## 2.2 Retrieval

A basic retrieval scheme takes as input the visual descriptor corresponding to the query image performed by the user and it computes the similarity between such a descriptor and all the visual descriptors of the database of features. As a result of the search, a ranked list of images is returned to the user. The list is ordered by a degree of similarity, that can be calculated in several ways [55]: Euclidean distance (that is the most used), Cosine similarity, Manhattan distance,  $\chi^2$ -square distance, etc [8].

## 2.3 Relevance Feedback

In some cases visual descriptors are not able to completely represent the image semantic content. Conse-

quently, the result of a CBIR system might be not completely satisfactory. One way to improve the performance is to allow the user to better specify its information need by expanding the initial query with other relevant images [50,27,66,32]. Once the result of the initial query is available, the feedback module makes it possible to automatically or manually select a subset of relevant images. In the case of automatic relevance feedback (*pseudo-relevance feedback*) [3], the top  $n$  images retrieved are considered relevant and used to expand the query. In the case of manual relevance feedback (*explicit relevance feedback (RF)*) [3], it is the user that manually selects  $n$  relevant of images from the results of the initial query. In both cases, the relevance feedback process can be iterated several times to better capture the information need. Given the initial query image and the set of relevant images, whatever they are selected, the feature extraction module computes the corresponding visual descriptors and the corresponding queries are performed individually. The final set of images is then obtained by combining the ranked sets of images that are retrieved. There are several alternative ways in which the relevance feedback could implemented to expand the initial query. Readers who would wish to deepen on this topic can refer the following papers [66,32,48].

The performance of the system when relevance feedback is used, strongly depends on the quality of the results achieved after the initial query. A system using effective features for indexing, returns a high number of relevant images in the first ranking positions. This makes the pseudo-relevance feedback effective and, in the case of manual relevance feedback, it makes easier to the user selecting relevant images within the result set.

Although there are several examples in the literature of manual RF [56,14,13], since human labeling task is enormously boring and time consuming, these schemes are not practical and efficient in a real scenario, especially when huge archives of images are considered. Apart from the pseudo-RF, other alternatives to manual RF approach are the hybrid systems such as the systems based on supervised machine learning [19,45]. This learning method aims at finding the most informative images in the archive that, when annotated and included in the set of relevant and irrelevant images (i.e., the training set), can significantly improve the retrieval performance [19,22]. The *Active-Learning-based RF* scheme presented by Demir et al. [19] is an example of hybrid scheme. Given a query, the user selects a small number of relevant and not relevant images that are used as training examples to train a binary classifier based on Support Vector Machines. The system

iteratively proposes images to the user that assigns the relevance feedback. At each RF iteration the classifier is re-trained using a set of images composed of the initial images and the images from the relevance feedback provided by the user. After some RF iterations, the classifier is able to retrieve images that are similar to the query with a higher accuracy with respect to the initial query. At each RF iteration, the system suggests images to the user by following this strategy: 1) the system selects the  $p$  most uncertain (i.e. ambiguous) images by taking the ones closest to the classifier hyperplanes; 2) the system selects the  $h$  (with  $h < p$ ) most diverse images from the highest density regions of the future space.

### 3 Methods and materials

Given an image database  $\mathcal{D}$  composed of  $M$  images, the most  $k$  relevant images of  $\mathcal{D}$  to a given query are the  $k$  images that have the smallest distances between their feature vectors and the feature vector extracted from the query image. Let us consider  $f^q$  and  $f^m$  as the feature vectors extracted from the query image and a generic image  $m$  of  $\mathcal{D}$  respectively. The euclidean distance function between them is defined as  $d(f^q, f^m) = \sqrt{\sum_{i=1}^L (f_i^q - f_i^m)^2}$ .  $L$  indicates the feature vector length.

In this work we evaluated:

1. several visual descriptors as described in Sect. 3.1;
2. different retrieval schemes as described in Sect. 3.2;

We conducted all the experiments on two publicly available datasets described in Sec. 3.3 for which the ground truth is known.

#### 3.1 Visual descriptors

In this work we compared visual descriptors for content-based retrieval of remote sensing images. We considered a few representative descriptors selected from global, local and Convolutional Neural Networks approaches. In some cases we considered both color and gray-scale images. The gray-scale image  $L$  is defined as follows:  $L = 0.299R + 0.587G + 0.114B$ . All feature vectors have been  $L^2$  normalized <sup>2</sup>:

##### 3.1.1 Global descriptors

- 256-dimensional gray-scale histogram (Hist L) [41];
- 512-dimensional Hue and Value marginal histogram obtained from the HSV color representation of the image (Hist H V) [41];

- 768-dimensional RGB and *rgb* marginal histograms (Hist RGB and Hist *rgb*) [46];
- 1536-dimensional spatial RGB histogram achieved from a RGB histogram calculated in different part of the image (Spatial Hist RGB) [41];
- 5-dimensional feature vector composed of contrast, correlation, energy, entropy and homogeneity extracted from the *co-occurrence matrices* of each color channel (Co-occ. matr.) [2,26];
- 144-dimensional *Color and Edge Directivity Descriptor* (CEDD) features. This descriptor uses a fuzzy version of the five digital filters proposed by the MPEG-7 Edge Histogram Descriptor (EHD), forming 6 texture areas. CEDD uses 2 fuzzy systems that map the colors of the image in a 24-color custom palette;
- 8-dimensional *Dual Tree Complex Wavelet Transform* features obtained considering four scales, mean and standard deviation, and three color channels (DT-CWT and DT-CWT L) [7,4];
- 512-dimensional *Gist* features obtained considering eight orientations and four scales for each channel (Gist RGB) [43];
- 32-dimensional *Gabor* features composed of mean and standard deviation of six orientations extracted at four frequencies for each color channel (Gabor L and Gabor RGB) [7,6];
- 264-dimensional *opponent Gabor* feature vector extracted as Gabor features from several inter/intra channel combinations: monochrome features extracted from each channel separately and opponent features extracted from couples of colors at different frequencies (Opp. Gabor RGB) [28];
- 580-dimensional *Histogram of Oriented Gradients* feature vector [30]. Nine histograms with nine bins are concatenated to achieve the final feature vector (HoG);
- 78-dimensional feature vector obtained calculating morphological operators (*granulometries*) at four angles and for each color channel (Granulometry) [24];
- 18-dimensional *Local Binary Patterns* (LBP) feature vector for each channel. We considered LBP applied to gray images and to color images represented in RGB [35]. We selected the LBP with a circular neighbourhood of radius 2 and 16 elements, and 18 uniform and rotation invariant patterns. We set  $w = 16$  and  $w = 30$  for the LandUse and SceneSat datasets respectively (LBP L and LBP RGB).

##### 3.1.2 Local descriptors

1. SIFT: We considered four variants of the *Bag of Visual Words* (BoVW) representation of a 128-dimensional

<sup>2</sup> The feature vector has been divided by its  $L^2$ -norm.

Scale Invariant Feature Transform (SIFT) calculated on the gray-scale image. For each variant, we built a codebook of 1024 visual words by exploiting images from external sources.

The four variants are:

- SIFT: 1024-dimensional BoVW of SIFT descriptors extracted from regions at given key points chosen using the SIFT detector (SIFT);
  - Dense SIFT: 1024-dimensional BoVW of SIFT descriptors extracted from regions at given key points chosen from a dense grid.
  - Dense SIFT (VLAD): 25 600-dimensional vector of locally aggregated descriptors (VLAD) [12].
  - Dense SIFT (FV): 40 960-dimensional Fisher’s vectors (FV) of locally aggregated descriptors [29].
2. LBP: We considered the *Bag of Visual Words* (BoVW) representation of Local Binary Patterns descriptor calculated on each channel of the RGB color space separately and then concatenated. LBP has been extracted from regions at given key points sampled from a dense grid every 16 pixels. We considered the LBP with a circular neighbourhood of radius 2 and 16 elements, and 18 uniform and rotation invariant patterns [16]. We set  $w = 16$  and  $w = 30$  for the LandUse and SceneSat respectively. Also in this case the codebook was built using an external dataset (Dense LBP RGB).

### 3.1.3 CNN-based descriptors

The CNN-based features have been obtained as the intermediate representations of deep convolutional neural networks originally trained for scene and object recognition. The networks are used to generate a visual descriptor by removing the final softmax nonlinearity and the last fully-connected layer. We selected the most representative CNN architectures in the state of the art [58] by considering a different accuracy/speed trade-off. All the CNNs have been trained on the ILSVRC-2012 dataset using the same protocol as in [31]. In particular we considered 4096, 2048, 1024 and 128-dimensional feature vectors as follows [47, 39]:

- *BVLC AlexNet* (BVLC AlexNet): this is the AlexNet trained on ILSVRC 2012 [31].
- *BVLC Reference CaffeNet* (BVLC Ref): a AlexNet trained on ILSVRC 2012, with a minor variation [58] from the version as described in [31].
- *Fast CNN* (Vgg F): it is similar to the one presented in [31] with a reduced number of convolutional layers and the dense connectivity between convolutional layers. The last fully-connected layer is 4096-dimensional [10].
- *Medium CNN* (Vgg M): it is similar to the one presented in [65] with a reduced number of filters in the convolutional layer four. The last fully-connected layer is 4096-dimensional [10].
- *Medium CNN* (Vgg M-2048-1024-128): three modifications of the Vgg M network, with lower dimensional last fully-connected layer. In particular we used a feature vector of 2048, 1024 and 128 size [10].
- *Slow CNN* (Vgg S): it is similar to the one presented in [52] with a reduced number of convolutional layers, less filters in the layer five and the Local Response Normalization. The last fully-connected layer is 4096-dimensional [10].
- *Vgg Very Deep 19 and 16 layers* (Vgg VeryDeep 16 and 19): the configuration of these networks has been achieved by increasing the depth to 16 and 19 layers, that results in a substantially deeper network than the ones previously [53].

## 3.2 Retrieval schemes

We evaluated and compared three retrieval schemes exploiting different distance functions, namely Euclidean, Cosine, Manhattan, and  $\chi^2$ -square and an active-learning-based RF scheme using the histogram intersection as distance measure. In particular, we considered:

1. *A basic IR*. This scheme takes a query as input and outputs a list of ranked similar images.
2. *Pseudo-RF*. This scheme considers the first  $n$  images returned after the initial query as relevant. We considered different values of  $n$  ranging between 1 and 10.
3. *Manual RF*. Since the ground truth is known, we simulated the human interaction by taking the first  $n$  actual relevant images from the result set obtained after the initial query. We evaluated performance at different values of  $n$  ranging between 1 and 10.
4. *Active-Learning-based RF*. We considered an Active-Learning-based RF scheme as presented by Demir et al. [19]. The RF scheme requires the interaction with the user that we simulated taking relevant and not relevant images from the ground-truth.

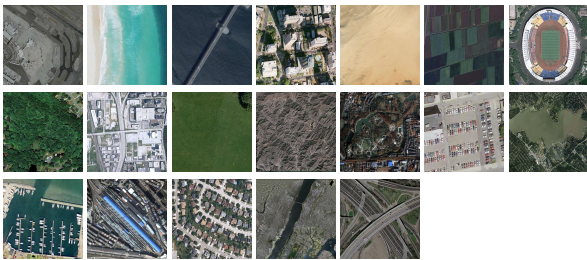
## 3.3 Remote Sensing Datasets

### 3.3.1 21-Class Land Use/Land Cover Dataset (LandUse)

This is a dataset of images of 21 land-use classes selected from aerial orthoimagery with a pixel resolution of 30 cm [62]. The images were downloaded from



**Fig. 2** Examples from the 21-Class Land-Use/Land-Cover dataset. From the top left to bottom right: *agricultural, airplane, baseball diamond, beach, buildings, chaparral, dense residential, forest, freeway, golf course, harbor, intersection, medium density residential, mobile home park, overpass, parking lot, river, runway, sparse residential, storage tanks, and tennis courts.*



**Fig. 3** Examples from the 19-Class Satellite Scene dataset. From the top left to bottom right: *airport, beach, bridge, commercial area, desert, farmland, football field, forest, industrial area, meadow, mountain, park, parking, pond, port, railway station, residential area, river and viaduct.*

the United States Geological Survey (USGS) National Map of some US regions.<sup>3</sup> For each class, one hundred  $256 \times 256$  RGB images are available for a total of 2100 images. The list of 21 classes is the following: *agricultural, airplane, baseball diamond, beach, buildings, chaparral, dense residential, forest, freeway, golf course, harbor, intersection, medium density residential, mobile home park, overpass, parking lot, river, runway, sparse residential, storage tanks, and tennis courts.* Some examples are shown in Fig. 2.

### 3.3.2 19-Class Satellite Scene (SceneSat)

This dataset consists of 19 classes of satellite scenes collected from Google Earth (Google Inc.)<sup>4</sup>. Each class has about fifty  $600 \times 600$  RGB images for a total of 1005 images [17,61]. The list of 19 classes is the following: *airport, beach, bridge, commercial area, desert, farmland, football field, forest, industrial area, meadow, mountain, park, parking, pond, port, railway station, residential area, river and viaduct.* An example of each class is shown in Fig. 3.

<sup>3</sup> <http://vision.ucmerced.edu/datasets>

<sup>4</sup> <http://dsp.whu.edu.cn/cn/staff/yw/HRSScene.html>

### 3.3.3 Differences between LandUse and SceneSat

The datasets used for the evaluation are quite different in terms of image size and resolution. LandUse images are of size  $256 \times 256$  pixels while SceneSat images are of size  $600 \times 600$  pixels. Fig. 4 displays some images from the same category taken from the two datasets. It is quite evident that the images taken from the LandUse dataset are at a different zoom level with respect to the images taken from the SatScene dataset. It means that objects in the LandUse dataset will be more easily recognizable than the objects contained in the SceneSat dataset, see the samples of *harbour* category in Fig. 4. The SceneSat images depict a larger land area than LandUse images. It means that the SceneSat images have a more heterogeneous content than LandUse images, see some samples from *harbour, residential area* and *parking* categories reported in Fig. 2 and Fig. 3. Due to these differences between the two considered datasets, we may expect that the same visual descriptors will have different performance across datasets, see Sec. 4.

## 3.4 Retrieval measures

Image retrieval performance has been assessed by using three state of the art measures: the *Average Normalized Modified Retrieval Rank* (ANMRR), *Precision* (Pr) and *Recall* (Re), *Mean Average Precision* (MAP) [38,37]. We also adopted the *Equivalent Query Cost* (EQC) to measure the cost of making a query independently of the computer architecture.

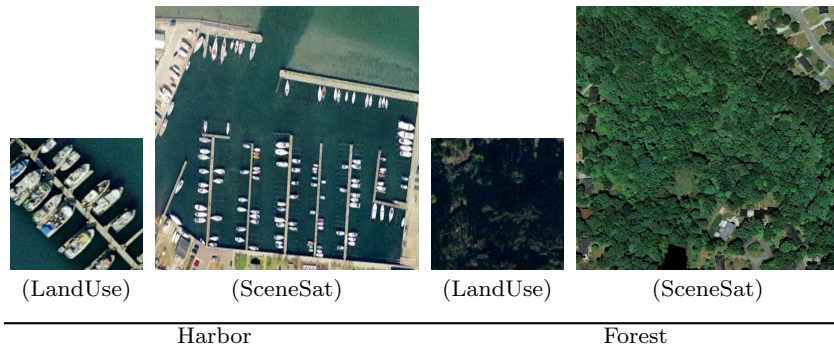
### 3.4.1 Average Normalized Modified Retrieval Rank (ANMRR)

The ANMRR measure is the MPEG-7 retrieval effectiveness measure commonly accepted by the CBIR community [37] and largely used by recent works on content-based remote sensing image retrieval [44,1,63]. This metric considers the number and rank of the relevant (ground truth) items that appear in the top images retrieved. This measure overcomes the problem related to queries with varying ground-truth set sizes. The ANMRR ranges in value between zero to one with lower values indicating better retrieval performance and is defined as follows:

$$ANMRR = \frac{1}{NQ} \sum_{q=1}^{NQ} \frac{AVR(q) - 0.5[1 + NG(q)]}{1.25K(q) - 0.5[1 + NG(q)]}.$$

$NQ$  indicates the number of queries  $q$  performed.  $NG(q)$  is the size of ground-truth set for each query  $q$ .  $K(q)$





**Fig. 4** Comparison between images of the same classes between LandUse and SceneSat dataset.

is a constant penalty that is assigned to items with a higher rank.  $K(q)$  is commonly chosen to be  $2NG(q)$ . AVR is the *Average Rank* for a single query  $q$  and is defined as

$$AVR(q) = \frac{1}{NG(q)} \sum_{k=1}^{NG(q)} Rank(k).$$

where  $Rank(k)$  is the  $k$ th position at which a ground-truth item is retrieved.  $Rank(k)$  is defined as:

$$Rank(k) = \begin{cases} Rank(k), & \text{if } Rank(k) \leq K(q) \\ 1.25K(q), & \text{if } Rank(k) > K(q). \end{cases}$$

### 3.4.2 Precision and Recall

Precision is the fraction of the images retrieved that are relevant to the query

$$Pr = \frac{|\{\# \text{ relevant images}\} \cap \{\# \text{ retrieved images}\}|}{|\{\# \text{ retrieved images}\}|}$$

It is often evaluated at a given cut-off rank, considering only the topmost  $k$  results returned by the system. This measure is called *precision at  $k$*  or  $Pr@k$ .

Recall is the fraction of the images that are relevant to the query that are successfully retrieved:

$$Re = \frac{|\{\# \text{ relevant images}\} \cap \{\# \text{ retrieved images}\}|}{|\{\# \text{ relevant images}\}|}$$

In a ranked retrieval context, precision and recall values can be plotted to give the *interpolated precision-recall curve* [38]. This curve is obtained by plotting the interpolated precision measured at the 11 recall levels of 0.0, 0.1, 0.2, ..., 1.0. The interpolated precision  $P_{interp}$  at a certain recall level  $k$  is defined as the highest precision found for any recall level  $k' \geq k$ :

$$P_{interp}(k) = \max_{k' \geq k} P(k')$$

### 3.4.3 Mean Average Precision (MAP)

Given a set of queries, *Mean Average Precision* is defined as,

$$MAP = \frac{\sum_{q=1}^Q AvePr(q)}{Q}.$$

where the average precision  $AvePr$  for each query  $q$  is defined as,

$$AvePr = \frac{\sum_{k=1}^n (Pr(k) \times rel(k))}{\# \text{ of relevant images}}$$

where  $k$  is the rank in the sequence of retrieved images,  $n$  is the number of retrieved images,  $Pr(k)$  is the precision at cut-off  $k$  in the list ( $Pr@k$ ), and  $rel(k)$  is an indicator function equalling 1 if the item at rank  $k$  is a relevant image, zero otherwise.

### 3.4.4 Equivalent Query Cost

Several previous works, such as [1], report a table that compares the computational time needed to execute a query when different indexing techniques have been used. This comparison can not be replicated because the computational time strictly depends on the computer architecture. To overcome this problem, we defined the *Equivalent Query Cost (EQC)* that measures the computational cost needed to execute a given query independently of the computer architecture. This measure is based on the fact that the calculation of the distance between two visual descriptors is linear in number of components and on the definition of *basic cost C*. The *basic cost* is defined as the amount of computational effort that is needed to execute a single query over the entire database  $\mathcal{D}$  when a visual descriptor of length  $B$  is used as indexing technique. The *EQC* of a generic visual descriptor of length  $L$  can be obtained as follows:

$$EQC = C \left\lceil \frac{L}{B} \right\rceil,$$

where the symbol  $\lfloor x \rfloor$  stands for the integer part of the number  $x$ , while  $B$  is set to 5, that corresponds to the length of the co-occurrence matrices, that is the shortest descriptor evaluated in the experiments presented in this work.

## 4 Results

### 4.1 Feature evaluation using the basic retrieval scheme

In this section we compare visual descriptors listed in Sec. 3.1 by using the basic retrieval scheme. In order to make the results more concise, in this section we show only the experiments performed employing the Euclidean distance. Given an image dataset, in turn, we used each image as query image and evaluated the results according to the metrics discussed above, i.e.  $ANMRR$ ,  $MAP$ ,  $P@5$ ,  $P@10$ ,  $P@50$ ,  $P@100$ ,  $P@1000$  and  $EQC$ . In the case of the LandUse dataset we performed 2100 queries while in the case of SatScene dataset we evaluated 1005 queries in total.

The results obtained on the LandUse dataset are showed in Table 1, while those obtained on the SatScene dataset are showed in Table 2. Regarding the LandUse dataset, the best results are obtained by using the CNN-based descriptors and in particular the Vgg M and Vgg S. The global descriptors have the lowest performance, with the co-occurrence matrices being the worst one. The local descriptors achieve better results than global descriptors but worse than CNN-based descriptors. In particular, the Vgg M, compared with Bag of Dense SIFT and DT-CWT, achieves an  $ANMRR$  value that is lower of about 20%, a  $MAP$  value that is higher of about 30%, a  $P@5$  that is higher of about 30%, a  $P@10$  value that is higher of about 30%. The same behavior can be observed for the remaining precision levels. In particular, looking at  $P@100$  we can notice that only the Vgg M descriptor is capable of retrieving about half of the existing images for each class ( $P@100 = 50.96$ ). Regarding the SatScene dataset, the best results are obtained by the CNN-based descriptors and in particular the BVLC Ref and Vgg F. The global descriptors have the lowest performance, with the co-occurrence matrices being the worst one. The local descriptors achieve better results than global descriptors but worse than CNN-based descriptors apart in the case of  $P@5$ . In particular the BVLC Ref, compared with Bag of Dense SIFT (FV), achieves an  $ANMRR$  value that is lower of about 10%, a  $MAP$  value that is higher of about 10%, a  $P@5$  that is lower of about 1%, a  $P@10$  value that is higher of about 5%. Similar behavior can be observed for the remaining precision levels. In particular, looking at  $P@50$  we can notice that only BVLC Ref is capable

of retrieving about half of the existing images for each class ( $P@50 = 49.75$ ).

The first columns of tables 9 and 10 show the best performing visual descriptor for each remote sensing image class. Regarding LandUse dataset, the CNN-based descriptors are the best in the retrieval of all classes apart from the class *dense residential* where the local descriptor SIFT performs better. The images of the *dense residential* class contain regular objects rotated and translated on the image plane and the SIFT descriptor is specially designed to handle these imaging conditions. Regarding the SceneSat dataset, both CNN-based and local descriptors works better than global descriptors apart the cases of the classes *desert* and *pond* where the DT-CWT performs better. Differently from the case of LandUse dataset, the CNN-descriptors work worse than local descriptors in many more classes. It depends from the fact that the SceneSat images depict a larger earth surface and then much more objects, see the images related to the classes *parking*, *river*, etc.

In Fig. 5 the *interpolated 11-points precision-recall* curves achieved by a selection of visual descriptors are plotted. It is clear that, in this experiments CNN-based descriptors outperform again other descriptors. It is interesting to note that in the case of SatScene dataset, local descriptors perform better than others when the recall level is very low. This depends on the fact that the SatScene dataset contains images with more textures and objects than the LandUse dataset (cfr. Figures 2 and 3) and local descriptors work better than others on these classes.

Concerning the computational cost, the Bag Dense SIFT (FV) is the most costly solution with the worst cost-benefit trade-off. Early after the Bag Dense SIFT (FV), the Vgg M is the other most costly descriptor that is about 200 more costly than the DT-CWT, that is among the global descriptors the best performing one.

One may prefer a less costly retrieval strategy that is less precise and then choose for the DT-CWT. Among the CNN-based descriptors, the Vgg M 128 has better  $ANMRR$  values than the DT-CWT for both datasets. The Vgg M 128 is six times more costly than DT-CWT. Concluding, the Vgg M 128 descriptor has the best cost-benefit trade-off.

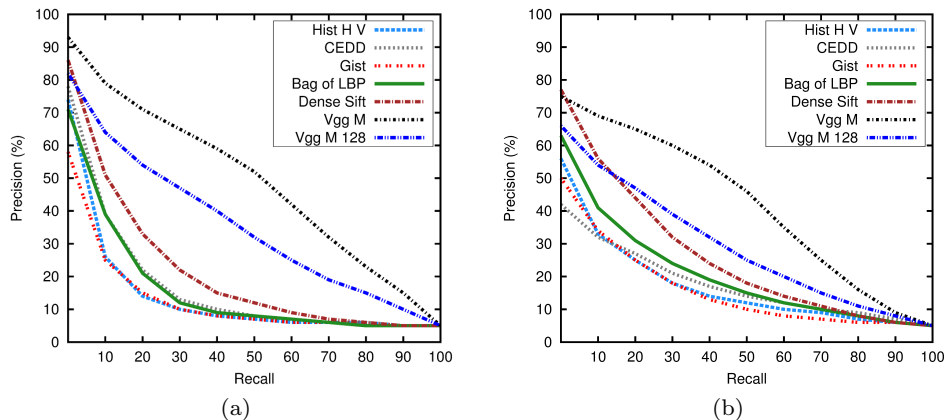
### 4.2 Feature evaluation using the pseudo-RF retrieval scheme

In the case of pseudo RF, we used the top  $n$  images retrieved after the initial query for re-querying the system. The computational cost of such a system is  $n$  times higher than the cost of a basic system.



Features	ANMRR	MAP	P@5	P@10	P@50	P@100	P@1000	EQC
<i>Global</i>								
Hist. L	0.816	12.46	36.65	30.17	18.07	13.74	5.96	51
Hist. H V	0.781	15.98	54.22	43.49	23.41	16.84	6.27	102
Hist. RGB	0.786	15.39	51.82	41.83	22.29	16.35	6.14	153
Hist. <i>rgb</i>	0.800	14.34	49.46	38.97	20.88	15.31	6.00	153
Spatial Hist. RGB	0.808	14.36	37.70	31.13	19.09	14.62	5.95	307
Co-occ. matr.	0.861	8.69	19.36	17.20	12.14	10.06	5.74	1
CEDD	0.736	19.89	62.45	52.39	29.54	20.86	6.49	28
DT-CWT L	0.707	21.04	39.64	36.36	26.81	22.11	7.90	1
DT-CWT	0.676	24.53	55.63	48.92	32.52	25.09	7.95	4
Gist RGB	0.781	17.65	45.94	38.97	23.10	17.01	6.09	102
Gabor L	0.766	16.08	44.60	37.28	22.65	17.63	7.11	6
Gabor RGB	0.749	18.06	52.72	44.48	25.71	19.13	7.04	19
Opp. Gabor RGB	0.744	18.76	53.81	44.89	26.18	19.69	6.99	52
HoG	0.751	17.85	48.67	41.88	25.37	19.12	6.18	116
Granulometry	0.779	15.45	39.36	33.31	20.76	16.30	7.15	15
LBP L	0.760	16.82	52.77	45.16	26.34	18.84	6.01	3
LBP RGB	0.751	17.96	58.73	49.83	28.12	19.62	6.07	10
<i>Local - BoVW</i>								
Dense LBP RGB	0.744	19.01	60.10	51.89	29.12	20.30	6.33	204
SIFT	0.635	28.49	53.56	49.40	35.98	28.42	8.26	204
Dense SIFT	0.672	25.44	72.30	62.61	35.51	25.96	7.12	204
Dense SIFT (VLAD)	0.649	28.01	74.93	65.25	38.20	28.10	7.18	5120
Dense SIFT (FV)	0.639	29.18	75.34	66.28	39.09	28.54	7.88	8192
<i>CNN-based</i>								
Vgg F	0.386	53.55	85.00	79.73	62.29	50.24	9.57	819
Vgg M	<b>0.378</b>	<b>54.44</b>	<b>86.16</b>	81.03	63.42	<b>50.96</b>	9.59	819
Vgg S	0.381	54.18	86.10	<b>81.18</b>	<b>63.46</b>	50.50	<b>9.60</b>	819
Vgg M 2048	0.388	53.16	85.04	80.26	62.77	50.14	9.52	409
Vgg M 1024	0.400	51.66	84.43	79.41	61.40	48.88	9.50	204
Vgg M 128	0.498	40.94	73.82	68.30	50.67	39.92	9.18	25
BVLC Ref	0.402	52.00	84.73	79.37	61.10	48.96	9.49	819
BVLC AlexNet	0.410	51.13	84.06	78.68	59.99	48.01	9.51	819
Vgg VeryDeep 16	0.394	52.46	83.91	78.34	61.38	49.78	9.60	819
Vgg VeryDeep 19	0.398	51.95	82.84	77.60	60.69	49.16	9.63	819

**Table 1** LandUse Dataset results obtained with a basic retrieval system with the Euclidean distance. The lower is the value of *ANMRR* and *EQC* the better is the performance. For the other metrics is the opposite. The best result is reported in bold.



**Fig. 5** Interpolated 11-points *precision-recall* curves of a selection of visual descriptors for each dataset. (a) LandUse. (b) SatScene.

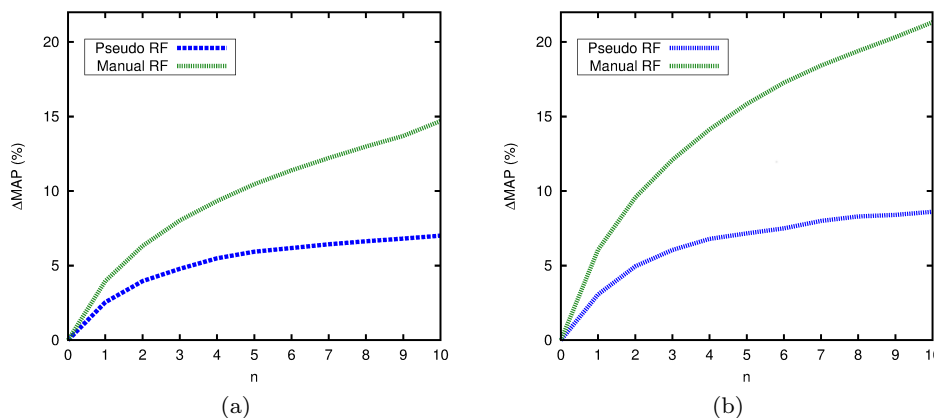
Results obtained choosing  $n = 5$  are showed in Table 3 and 4 for the LandUse and SatScene datasets respectively. It can be noticed that, in both cases, the employment of the pseudo RF scheme gives an improvement with respect to the basic retrieval system whatever is the visual descriptor employed. The CNN-based and local descriptors that, when used in a basic system,

obtained the highest precision at level 5 ( $Pr@5$ ), have the largest improvement of performance.

Figures 6(a) and (b) show the difference of MAP between the pseudo RF scheme and the basic retrieval scheme, when the Vgg visual descriptor is employed. The value  $n$  ranges from 0 (that corresponds to the basic system) to 10. It can be noticed that the improvement of performance, when  $n$  is equal to 5, is of about

Features	ANMRR	MAP	P@5	P@10	P@50	P@100	P@1000	EQC
<i>Global</i>								
Hist. L	0.728	19.86	37.69	32.61	21.05	15.98	5.21	51
Hist. H V	0.704	23.23	43.98	37.29	23.10	17.05	5.21	102
Hist. RGB	0.722	21.24	40.96	34.71	21.17	16.30	5.20	153
Hist. <i>rgb</i>	0.702	23.03	43.76	37.87	23.31	17.11	5.21	153
Spatial Hist. RGB	0.720	22.21	38.85	33.36	21.81	16.30	5.21	307
Co-occ. matr.	0.822	11.73	21.25	18.16	12.94	11.00	5.19	1
CEDD	0.684	24.15	38.13	34.77	24.65	18.52	5.20	28
DT-CWT L	0.672	23.48	35.90	32.43	24.32	20.20	5.21	1
DT-CWT	0.581	33.16	51.00	45.98	32.99	24.52	5.21	4
Gist RGB	0.706	22.98	41.73	37.31	22.98	16.81	5.19	102
Gabor L	0.685	22.84	40.82	35.63	23.45	19.07	5.21	6
Gabor RGB	0.649	27.00	49.19	43.42	26.92	20.70	5.20	19
Opp. Gabor RGB	0.638	28.08	48.14	42.48	28.61	21.01	5.20	52
HoG	0.724	19.97	40.24	35.31	21.73	15.82	5.20	16
Granulometry	0.717	21.41	39.20	33.60	20.78	17.22	5.21	15
LBP L	0.690	22.61	47.24	40.55	24.06	18.16	5.20	48
LBP RGB	0.664	24.95	50.33	43.98	26.33	19.40	5.20	10
<i>Local - BoVW</i>								
Dense LBP RGB	0.660	24.81	51.12	44.29	26.55	19.67	5.21	204
SIFT	0.559	35.47	59.40	53.22	35.04	25.49	5.20	204
Dense SIFT	0.603	31.29	64.06	55.80	31.70	22.24	5.20	204
Dense SIFT (VLAD)	0.552	35.89	71.30	62.78	36.19	25.03	5.20	5120
Dense SIFT (FV)	0.518	39.44	<b>72.34</b>	64.69	38.84	27.23	5.20	8192
<i>CNN-based</i>								
Vgg F	0.408	49.91	71.52	<b>68.98</b>	49.62	33.07	5.21	819
Vgg M	0.419	48.59	71.50	68.27	48.62	32.45	5.21	819
Vgg S	0.416	48.89	71.46	68.62	48.79	32.58	5.20	819
Vgg M 2048	0.431	47.14	71.08	67.52	47.33	31.83	5.21	409
Vgg M 1024	0.443	45.86	70.51	66.61	46.05	31.23	5.21	204
Vgg M 128	0.551	34.54	59.30	54.08	36.05	25.65	5.20	25
BVLC Ref	<b>0.407</b>	<b>50.04</b>	71.22	68.65	<b>49.75</b>	<b>33.15</b>	<b>5.21</b>	819
BVLC AlexNet	0.421	48.52	70.45	66.91	48.22	32.51	5.20	819
Vgg VeryDeep 16	0.440	46.18	70.67	66.71	46.22	31.46	5.20	819
Vgg VeryDeep 19	0.455	44.34	69.17	64.65	44.84	30.66	5.20	819

**Table 2** SatScene dataset results obtained with a basic retrieval system with the Euclidean distance. The lower is the value of *ANMRR* and *EQC* the better is the performance. For the other metrics is the opposite. The best result is reported in bold.



**Fig. 6** Difference of performance ( $\Delta MAP$ ), when the Vgg M is employed, between the pseudo RF and the basic retrieval system, and between manual RF and the basic retrieval system. (a) LandUse. (b) SceneSat.

5% in the case of LandUse and of about 7% in the case of SceneSat dataset.

The second columns of tables 9 and 10 show the best performing visual descriptor for each remote sensing image class. In both cases, LandUse and SceneSat, the best performing visual descriptors are quite the same as in the case of the basic retrieval system.

### 4.3 Feature evaluation using the manual-RF retrieval scheme

In manual RF, we used the first  $n$  actually relevant images retrieved after the initial query for re-querying the system. The computational cost of such a system is  $n$  times higher than the cost of a basic system. The first five relevant images appear, in the worst case (co-

features	ANMRR	MAP	P@5	P@10	P@50	P@100
<i>Global</i>						
Hist. L	0.820	12.31	35.16	28.78	17.42	13.43
Hist. H V	0.783	15.94	53.16	42.82	23.03	16.62
Hist. RGB	0.789	15.37	51.41	41.22	21.89	16.10
Hist. <i>rgb</i>	0.804	14.16	48.09	37.01	20.19	14.93
Spatial Hist. RGB	0.824	13.87	35.15	27.60	16.96	13.27
Co-occ. matr.	0.863	8.56	19.02	16.68	11.88	9.87
CEDD	0.740	19.88	62.27	52.58	29.25	20.55
DT-CWT L	0.708	21.03	39.50	35.67	26.67	22.04
DT-CWT	0.677	24.59	55.13	48.30	32.24	25.00
Gist RGB	0.804	17.14	44.09	35.79	20.46	15.12
Gabor L	0.769	15.92	44.14	36.39	22.16	17.38
Gabor RGB	0.750	18.04	52.56	44.00	25.53	18.97
Opp. Gabor RGB	0.748	18.62	53.73	44.48	25.78	19.32
HoG	0.757	17.79	47.73	40.51	24.69	18.61
Granulometry	0.783	15.26	38.54	31.92	20.29	16.00
LBP L	0.762	16.82	52.23	44.32	26.25	18.61
LBP RGB	0.752	18.06	58.35	49.75	28.16	19.53
<i>Local - BoVW</i>						
Dense LBP RGB	0.747	19.09	59.49	50.99	28.76	20.17
SIFT	0.648	28.56	52.97	47.53	34.65	27.39
Dense SIFT	0.675	25.67	72.20	62.46	35.14	25.75
Dense SIFT (VLAD)	0.652	28.42	74.98	64.82	37.73	27.77
Dense SIFT (FV)	0.652	28.42	74.98	64.82	37.73	27.77
<i>CNN-based</i>						
Vgg F	0.360	57.22	85.29	80.91	65.26	52.88
Vgg M	<b>0.344</b>	<b>58.83</b>	<b>86.55</b>	<b>82.73</b>	67.11	<b>54.26</b>
Vgg S	0.350	58.34	86.42	82.58	66.81	53.50
Vgg M 2048	0.348	58.27	85.63	82.21	<b>67.21</b>	53.82
Vgg M 1024	0.358	56.99	85.27	81.79	66.03	52.92
Vgg M 128	0.470	44.46	74.04	69.85	53.60	42.39
BVLC Ref	0.376	55.46	84.84	80.77	63.79	51.34
BVLC AlexNet	0.388	54.31	84.13	79.37	62.18	50.05
Vgg VeryDeep 16	0.365	56.30	84.25	79.88	64.36	52.50
Vgg VeryDeep 19	0.369	55.80	83.42	79.08	63.71	51.99

**Table 3** LandUse dataset results obtained with the Pseudo RF scheme with the Euclidean distance. The lower is the value of *ANMRR* and *EQC* the better is the performance. For the other metrics is the opposite. The best result is reported in bold.

occurrence matrix), within the top 50 images, while in the best case (Vgg M), within the top 10 (cfr. table 1).

Results obtained choosing  $n = 5$  are showed in Table 5 and 6 for the LandUse and SatScene datasets respectively. It can be noticed that, in both cases, the employment of the manual RF scheme gives an improvement with respect to both the basic retrieval and the pseudo RF systems. The CNN-based and local descriptors that, when used in a basic system, obtained the highest precision at level 5 ( $Pr@5$ ), have also in this case the largest improvement of performance.

Figures 6(a) and (b) show the difference between the MAP of the manual RF scheme and the basic retrieval scheme, when the Vgg visual descriptor is employed, The value  $n$  ranges from 0 (that corresponds to the basic system) to 10. It can be noticed that for both datasets the improvement of performance is, when  $n$  is equal to 5, of about 9% in the case of LandUse and of about 14% in the case of SceneSat. The manual RF scheme, when  $n$  is equal to 1, achieves the same performance of the pseudo RF when  $n$  is equal to 2.

The third columns of tables 9 and 10 show the best performing visual descriptor for each remote sensing image class. In both cases, LandUse and SceneSat, the best performing visual descriptors are quite the same as in the cases of the basic and pseudo-RF retrieval system.

features	ANMRR	MAP	P@5	P@10	P@50	P@100
<i>Global</i>						
Hist. L	0.732	19.73	36.82	31.14	20.49	15.85
Hist. H V	0.713	23.04	42.77	35.80	22.36	16.56
Hist. RGB	0.725	21.34	40.84	33.99	20.85	16.17
Hist. <i>rgb</i>	0.716	22.62	42.73	35.91	22.08	16.43
Spatial Hist. RGB	0.742	21.55	36.92	30.25	19.77	15.14
Co-occ. matr.	0.825	11.57	21.00	17.64	12.72	10.85
CEDD	0.696	23.83	37.71	33.69	23.71	17.77
DT-CWT L	0.677	23.07	35.22	30.87	23.82	19.95
DT-CWT	0.586	33.01	50.65	45.09	32.54	24.23
Gist RGB	0.728	22.66	40.06	34.00	21.40	15.54
Gabor L	0.692	22.38	39.52	33.86	22.84	18.81
Gabor RGB	0.656	26.62	48.60	42.22	26.28	20.37
Opp. Gabor RGB	0.647	27.77	47.54	41.31	27.85	20.52
HoG	0.733	19.81	38.75	34.10	20.96	15.38
Granulometry	0.722	21.07	38.35	32.31	20.19	17.02
LBP L	0.701	22.12	46.43	38.80	23.09	17.50
LBP RGB	0.672	24.70	49.35	42.85	25.62	19.03
<i>Local - BoVW</i>						
Dense LBP RGB	0.669	24.31	50.43	42.40	25.72	19.31
SIFT	0.570	35.64	58.55	51.11	34.25	24.84
Dense SIFT	0.606	31.91	63.50	54.86	31.65	22.11
Dense SIFT (VLAD)	0.554	37.06	70.93	61.99	36.36	24.85
Dense SIFT (FV)	0.523	40.19	71.74	63.37	38.36	27.00
<i>CNN-based</i>						
Vgg F	0.372	54.18	72.08	70.39	53.50	34.85
Vgg M	0.383	52.91	<b>72.22</b>	70.31	52.57	34.16
Vgg S	0.381	53.13	72.18	70.45	52.65	34.24
Vgg M 2048	0.386	52.38	71.72	69.83	52.21	34.02
Vgg M 1024	0.398	51.08	70.95	69.12	50.83	33.46
Vgg M 128	0.519	38.16	60.00	56.65	39.14	27.34
BVLC Ref	<b>0.371</b>	<b>54.43</b>	72.00	<b>70.58</b>	<b>53.57</b>	<b>34.88</b>
BVLC AlexNet	0.391	52.44	70.77	68.65	51.56	34.07
Vgg VeryDeep 16	0.402	50.55	71.44	69.18	50.26	33.28
Vgg VeryDeep 19	0.419	48.61	70.01	67.17	48.58	32.48

**Table 4** SceneSat dataset results obtained with the Pseudo RF scheme with the Euclidean distance. The lower is the value of *ANMRR* and *EQC* the better is the performance. For the other metrics is the opposite. The best result is reported in bold.

#### 4.4 Feature evaluation using the active-learning-based-RF retrieval scheme

We considered the Active-Learning-based RF scheme as presented by Demir et al. [19]. As suggested by the original authors, we considered the following parameters: 10 RF iterations; an initial training set made of 2 relevant and 3 not relevant images;  $p = 20$  ambiguous images;  $h = 5$  diverse images; the histogram intersection as measure of similarity between feature vectors. The histogram intersection distance is defined as follows:

$$HI(f^n, f^m) = \sum_{l=1}^L \min(f_l^n, f_l^m),$$

where  $f^n$  and  $f^m$  are the feature vectors of two generic images and  $L$  is the size of the feature vector.

Results are showed in Table 7 and 8 for the LandUse and SatScene datasets respectively. Regarding the LandUse dataset, it can be noticed that the employment of the this RF scheme gives an improvement with respect to the other retrieval schemes for all the visual descriptors. In the case of CNN-based descriptors the improvement is of about 20%. Surprisingly, in the case of SceneSat dataset, the employment of the Active-Learning-based RF scheme gives a performance improvement only in the cases of global and local descriptors. In the best case, that is Bag of Dense SIFT (FV) the improvement

features	ANMRR	MAP	P@5	P@10	P@50	P@100
<i>Global</i>						
Hist. L	0.798	15.02	71.40	48.34	21.13	15.24
Hist. H V	0.762	18.52	83.90	59.44	26.51	18.39
Hist. RGB	0.771	17.73	80.50	57.16	25.06	17.65
Hist. <i>rgb</i>	0.782	16.73	79.96	54.60	23.80	16.66
Spatial Hist. RGB	0.789	17.47	82.30	52.48	22.59	16.15
Co-occ. matr.	0.853	9.76	38.02	28.78	14.02	10.74
CEDD	0.722	22.23	87.97	66.76	32.28	22.04
DT-CWT L	0.691	23.19	65.54	50.27	29.25	23.32
DT-CWT	0.654	27.21	80.47	62.06	35.64	26.85
Gist RGB	0.767	20.40	84.43	57.66	26.08	18.12
Gabor L	0.754	17.99	71.10	51.05	24.59	18.57
Gabor RGB	0.734	20.11	77.10	56.96	28.26	20.32
Opp. Gabor RGB	0.732	20.80	80.10	58.71	28.55	20.73
HoG	0.733	20.49	78.10	57.23	28.59	20.52
Granulometry	0.770	17.28	67.09	47.36	22.82	17.10
LBP L	0.746	18.91	77.58	57.98	29.05	19.98
LBP RGB	0.737	20.08	82.13	62.40	30.86	20.80
<i>Local - BoVW</i>						
Dense LBP RGB	0.727	21.74	88.73	66.33	32.21	21.76
SIFT	0.602	32.89	88.78	67.16	40.66	31.04
Dense SIFT	0.649	28.38	93.43	75.42	38.82	27.86
Dense SIFT (VLAD)	0.623	31.18	94.79	77.60	41.74	30.13
Dense SIFT (FV)	0.623	31.18	94.79	77.60	41.74	30.13
<i>CNN-based</i>						
Vgg F	0.329	60.53	97.39	89.99	69.47	55.64
Vgg M	<b>0.316</b>	<b>61.85</b>	97.82	91.13	70.93	56.64
Vgg S	0.320	61.45	97.58	90.98	70.77	56.04
Vgg M 2048	0.316	61.76	<b>97.97</b>	<b>91.20</b>	<b>71.58</b>	<b>56.66</b>
Vgg M 1024	0.326	60.55	97.78	90.83	70.48	55.73
Vgg M 128	0.422	49.53	95.30	83.89	59.85	46.46
BVLC Ref	0.347	58.63	97.50	89.95	67.71	53.91
BVLC AlexNet	0.357	57.63	97.26	88.90	66.53	52.72
Vgg VeryDeep 16	0.331	60.05	97.24	89.45	68.98	55.48
Vgg VeryDeep 19	0.334	59.56	96.97	88.88	68.39	54.92

**Table 5** LandUse dataset results obtained with the Manual RF scheme with the Euclidean distance. The lower is the value of *ANMRR* and *EQC* the better is the performance. For the other metrics is the opposite. For each row the best result is reported in bold.

is of about 40%. Performance decreases of about 40% in the case of CNN-based descriptors.

The fourth columns of tables 9 and 10 show the best performing visual descriptor for each remote sensing image class. In the case of LandUse dataset, the best performing visual descriptors are the CNN-based descriptors, while in the case of SceneSat dataset, the best performing are the local descriptors apart from a few number of classes.

#### 4.5 Average rank of visual descriptors across RS datasets

In table 11 we show the average rank of all the visual descriptors evaluated. The average rank is represented in the last column and obtained by averaging the ranks achieved by each visual descriptor across datasets, retrieval schemes and measures: *ANMRR*, *MAP*, *Pr* at 5,10,50,100 levels, and *EQC*. For sake of completeness, for each retrieval scheme, we displayed the average *ANMRR* across datasets and the *EQC* for each visual descriptor. From this table is quite clear that across datasets, the best performing visual descriptors are the CNN-based ones. The first 7 positions out of 32 are occupied by CNN-based descriptors. The global descriptor DT-CWT is at 8th position mostly because of the length of the vector that is very short. After

features	ANMRR	MAP	P@5	P@10	P@50	P@100
<i>Global</i>						
Hist. L	0.698	24.02	67.76	47.75	23.30	17.22
Hist. H V	0.670	28.17	78.95	55.00	25.93	18.30
Hist. RGB	0.686	25.91	72.36	51.58	24.09	17.77
Hist. <i>rgb</i>	0.675	27.44	76.54	54.10	25.35	18.12
Spatial Hist. RGB	0.682	28.06	83.62	54.21	24.86	17.71
Co-occ. matr.	0.803	14.04	41.59	30.37	14.59	11.52
CEDD	0.653	29.59	75.30	54.08	27.26	19.60
DT-CWT L	0.648	26.88	62.55	45.02	26.21	21.13
DT-CWT	0.544	37.90	78.35	59.78	36.08	26.13
Gist RGB	0.660	29.42	83.10	56.85	27.20	18.60
Gabor L	0.663	26.39	68.52	48.85	25.20	19.86
Gabor RGB	0.622	31.02	77.15	57.26	29.28	21.74
Opp. Gabor RGB	0.610	32.29	76.50	57.07	30.94	22.03
HoG	0.688	24.93	72.06	52.61	24.88	17.15
Granulometry	0.701	24.55	67.02	46.41	22.07	17.63
LBP L	0.655	27.47	79.06	56.44	27.07	19.57
LBP RGB	0.628	29.79	78.91	58.92	29.37	20.93
<i>Local - BoVW</i>						
Dense LBP RGB	0.625	29.82	83.16	59.42	29.55	21.11
SIFT	0.508	42.25	89.27	68.54	39.56	27.79
Dense SIFT	0.554	37.83	90.55	71.12	36.35	24.38
Dense SIFT (VLAD)	0.493	43.48	94.37	77.44	41.69	27.70
Dense SIFT (FV)	0.493	43.48	<b>94.37</b>	77.44	41.69	27.70
<i>CNN-based</i>						
Vgg F	0.330	59.44	92.22	80.82	57.44	36.75
Vgg M	0.340	58.30	92.36	81.06	56.41	36.10
Vgg S	0.336	58.69	92.42	81.15	56.74	36.34
Vgg M 2048	0.339	58.46	92.78	81.52	56.65	36.12
Vgg M 1024	0.349	57.21	92.78	80.85	55.31	35.73
Vgg M 128	0.448	46.57	90.89	74.01	45.39	30.70
BVLC Ref	<b>0.327</b>	<b>59.89</b>	92.38	<b>81.55</b>	<b>57.63</b>	<b>36.80</b>
BVLC AlexNet	0.343	58.26	92.72	80.74	55.97	36.16
Vgg VeryDeep 16	0.359	55.99	92.12	79.91	54.07	35.24
Vgg VeryDeep 19	0.368	54.79	91.84	79.23	53.23	34.76

**Table 6** SceneSat dataset results obtained with the Manual RF scheme with the Euclidean distance. The lower is the value of *ANMRR* and *EQC* the better is the performance. For the other metrics is the opposite. For each row the best result is reported in bold.

some other CNN-based descriptors, we find the local descriptors that despite their good performance, they are penalized by the size of the vector of feature that is very long, in the case of Dense SIFT (FV) is 40960 that is 2048 times higher than the size of DT-CWT.

Looking at the *EQC* columns of each retrieval schemes of table 11, it is quite evident that the use of Active-Learning-based RF is not always convenient. For instance, in the case of the top 5 visual descriptors of the table, the Active-Learning-based RF achieves globally worse performance than pseudo-RF with a much more higher *EQC*. This is not true in all other cases, where the performance achieved with the Active-Learning-based RF is better than pseudo-RF.

#### 4.6 Comparison with the state of the art

According to our results, one of the best performing visual descriptor is the Vgg M, while the best visual descriptor, when the computational cost is taken into account, is the Vgg M 128. We compared these descriptors, coupled with the four scheme described in Sec. 3.2, with some recent methods [1, 44, 63]. All these works used the basic retrieval scheme and the experiments have been conducted on the LandUse dataset. *Aptoula* proposed several global morphological texture descriptors [1]. *Ozkan* et al. used bag of visual words

features	ANMRR	MAP	P@5	P@10	P@50	P@100
<i>Global</i>						
Hist. L	0.753	19.18	71.46	52.51	25.23	18.82
Hist. H V	0.688	25.57	87.31	70.88	34.65	24.31
Hist. RGB	0.747	20.12	80.07	61.73	27.77	19.50
Hist. <i>rgb</i>	0.712	23.25	83.35	63.96	30.50	22.22
Spatial Hist. RGB	0.695	25.27	84.49	64.50	32.39	23.52
Coocc. matr.	0.851	10.28	32.18	24.41	13.94	10.94
CEDD	0.719	22.72	85.49	68.70	32.43	21.94
DT-CWT L	0.757	18.78	56.10	42.78	24.67	18.81
DT-CWT	0.698	24.48	77.90	63.52	33.58	23.73
Gist RGB	0.662	27.76	87.06	70.17	37.91	27.11
Gabor L	0.748	19.19	61.67	44.56	23.95	18.61
Gabor RGB	0.709	23.43	69.60	53.30	30.05	22.74
Opp. Gabor RGB	0.634	29.78	82.34	66.71	39.40	29.42
HoG	0.681	26.18	84.70	68.10	36.06	25.20
Granulometry	0.833	14.39	54.11	36.23	16.92	12.76
LBP L	0.791	16.82	64.78	47.73	24.17	16.49
LBP RGB	0.793	16.77	69.43	51.66	24.26	16.41
<i>Local - BoVW</i>						
Dense LBP RGB	0.726	22.41	85.21	68.24	31.99	21.34
SIFT	0.572	35.40	80.31	65.13	44.08	34.64
Dense SIFT	0.631	32.09	90.27	76.93	41.81	29.82
Dense SIFT (VLAD)	0.598	34.39	88.87	76.44	43.70	31.92
Dense SIFT (FV)	0.465	48.38	98.58	92.97	61.48	44.70
<i>CNN-based</i>						
Vgg F	0.256	69.33	<b>99.70</b>	97.47	79.92	63.90
Vgg M	<b>0.247</b>	<b>71.09</b>	99.39	<b>98.09</b>	<b>82.98</b>	<b>65.54</b>
Vgg S	0.260	69.45	99.34	96.42	79.88	63.61
Vgg M 2048	0.248	70.54	98.51	96.27	80.43	65.05
Vgg M 1024	0.266	68.22	99.09	96.84	78.75	62.73
Vgg M 128	0.333	60.72	97.70	94.03	73.60	56.17
BVLC Ref	0.292	66.05	98.70	95.98	76.56	60.72
BVLC AlexNet	0.281	66.98	99.49	96.77	77.36	61.58
Vgg VeryDeep 16	0.292	66.05	98.70	95.98	76.56	60.72
Vgg VeryDeep 19	0.292	66.05	98.70	95.98	76.56	60.72

**Table 7** LandUse dataset results obtained with the Active-Learning-based RF scheme. The lower is the value of *ANMRR* and *EQC* the better is the performance. For the other metrics is the opposite. For each row the best result is reported in bold.

(BoVW) descriptors, the vector of locally aggregated descriptors (VLAD) and the quantized VLAD (VLAD-PQ) descriptors [44]. Yang et al. [63] investigated the effects of a number of design parameters on the BoVW representation. They considered: saliency-versus grid-based local feature extraction, the size of the visual codebook, the clustering algorithm used to create the codebook, and the dissimilarity measure used to compare the BOVW representations.

The results of the comparison are shown in Table 12. The Bag of Dense SIFT (VLAD) presented in [44] achieves performance that is close to the CNN-based descriptors. This method achieves *ANMRR* = 0.460 with *EQC* = 5120. This result has been obtained considering a codebook built by using images from the LandUse dataset. Concerning the computational cost, the texture features [63,1] are better than Vgg M and Vgg M 128. In terms of trade-off between performance and computational cost, the Vgg M 128 descriptor achieves a *ANMRR* value that is about 25% lower than the one achieved by the CCH+RIT+FPS<sub>1</sub>+FPS<sub>2</sub> descriptor used in [1] with a computational cost that is about 2 times higher.

features	ANMRR	MAP	P@5	P@10	P@50	P@100
<i>Global</i>						
Hist. L	0.648	28.93	67.96	52.19	27.10	20.01
Hist. H V	0.574	36.02	76.44	61.02	34.64	23.78
Hist. RGB	0.646	29.86	74.03	57.51	28.50	19.43
Hist. <i>rgb</i>	0.587	35.72	76.70	62.33	33.68	22.71
Spatial Hist. RGB	0.549	38.34	80.78	64.05	36.62	25.10
Coocc. matr.	0.804	14.72	42.03	31.14	14.93	11.25
CEDD	0.673	27.15	69.53	53.37	26.10	18.20
DT-CWT L	0.688	25.51	55.14	42.37	23.85	18.12
DT-CWT	0.571	37.60	71.54	57.35	35.32	23.91
Gist RGB	0.551	38.50	88.12	70.45	36.75	24.55
Gabor L	0.672	26.71	65.65	46.94	24.21	19.31
Gabor RGB	0.612	32.21	70.51	55.46	30.40	22.13
Opp. Gabor RGB	0.473	46.13	86.77	74.32	44.11	29.00
HoG	0.699	24.17	73.53	53.95	23.91	16.37
Granulometry	0.794	18.23	53.31	37.13	15.88	11.59
LBP L	0.669	26.62	72.44	54.86	26.68	18.24
LBP RGB	0.667	27.26	65.65	49.47	26.07	19.14
<i>Local - BoVW</i>						
Dense LBP RGB	0.534	39.84	84.20	68.96	37.18	26.25
SIFT	0.473	46.13	89.61	76.34	43.64	29.25
Dense SIFT	0.455	48.71	92.30	80.85	45.83	29.47
Dense SIFT (VLAD)	0.396	54.98	91.98	84.73	50.72	33.14
Dense SIFT (FV)	<b>0.301</b>	<b>65.81</b>	<b>97.31</b>	<b>94.01</b>	<b>60.48</b>	<b>37.57</b>
<i>CNN-based</i>						
Vgg F	0.520	44.87	83.66	68.39	41.36	25.67
Vgg M	0.503	46.40	84.82	70.47	42.82	26.35
Vgg M 128	0.558	39.27	81.57	67.82	37.05	23.81
Vgg S	0.479	48.61	84.90	72.35	44.81	27.90
Vgg M 2048	0.467	48.85	84.60	72.33	46.05	28.59
Vgg M 1024	0.468	48.55	85.57	72.21	45.58	28.61
BVLC Ref	0.522	44.41	82.75	68.66	41.30	25.38
BVLC AlexNet	0.506	46.57	82.67	69.22	42.32	26.41
Vgg VeryDeep 16	0.505	46.77	86.97	72.49	42.40	26.27
Vgg VeryDeep 19	0.498	46.83	82.53	70.32	43.55	26.59

**Table 8** SceneSat dataset results obtained with the Active-Learning-based RF scheme. The lower is the value of *ANMRR* and *EQC* the better is the performance. For the other metrics is the opposite. For each row the best result is reported in bold.

## 5 Conclusions

In this work we presented an extensive evaluation of visual descriptors for content-based retrieval of remote sensing images. We evaluated global, local and Convolutional Neural Networks features coupled with four different content-based retrieval (CBIR) schemes: a basic CBIR, a pseudo relevance feedback (RF), a manual RF and an active-learning-based RF. The experimentation has been conducted on two publicly available datasets that are different in terms of image size and resolution. Results demonstrated that:

- CNN-based descriptors proved to perform better, on average, than global and local descriptors whatever is the retrieval scheme adopted and on both the datasets considered, see the summary table 11;
- Local descriptors demonstrated to perform better than global and CNN-based descriptors on those images that contain fine-grained textures and objects. This is true specially for the SceneSat dataset where local descriptors demonstrate to work better than other descriptors on classes like: mountain, park, parking, etc. See the tables 9 and 10;
- Pseudo and manual relevance feedback schemes demonstrated to be very effective only when coupled with a visual descriptor that is high performing in a basic retrieval system, such as CNN-based and local

descriptors. This is quite evident looking at 6a and b,

- Active-Learning-based RF demonstrated to be very effective on average and the best performing among retrieval schemes. The computational cost required to perform one query is, on average, at least 4 times higher than the computational cost required to perform a query with the other considered RF schemes and at least 20 times higher than a basic retrieval scheme.

As future works, it would be interesting to fine tune a pre-trained CNN on images from the RS domain and use the resulting features as visual descriptors as it has been done in the paper by Castelluccio et al. [9] for remote sensing image classification. To this end a new dataset of RS images that contains examples of images belonging to the classes of both the datasets considered in this paper is needed.

## Acknowledgments

The author is grateful to Prof. Raimondo Schettini for the valuable comments and stimulating discussions. We gratefully acknowledge the support of NVIDIA Corporation with the donation of the Tesla K40 GPU used for part of this research.










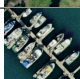









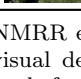
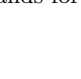
## References

1. Aptoula, E.: Remote sensing image retrieval with global morphological texture descriptors. *Geoscience and Remote Sensing, IEEE Transactions on* **52**(5), 3023–3034 (2014)
2. Arvis, V., Debain, C., Berducat, M., Benassi, A.: Generalization of the cooccurrence matrix for colour images: Application to colour texture. *Image Analysis & Stereology* **23**(1) (2004)
3. Baeza-Yates, R., Ribeiro-Neto, B., et al.: *Modern information retrieval*, vol. 463. ACM press New York (1999)
4. Barilla, M., Spann, M.: Colour-based texture image classification using the complex wavelet transform. In: *Electrical Engineering, Computing Science and Automatic Control, 2008. CCE 2008. 5th International Conference on*, pp. 358–363 (2008)
5. Bianco, S., Mazzini, D., Pau, D., Schettini, R.: Local detectors and compact descriptors for visual search: A quantitative comparison. *Digital Signal Processing* **44**, 1–13 (2015)
6. Bianconi, F., Fernández, A.: Evaluation of the effects of gabor filter parameters on texture classification. *Pattern Recognition* **40**(12), 3325–3335 (2007). DOI 10.1016/j.patcog.2007.04.023
7. Bianconi, F., Harvey, R., Southam, P., Fernández, A.: Theoretical and experimental comparison of different approaches for color texture classification. *Journal of Electronic Imaging* **20**(4) (2011)
8. ten Brinke, W., Squire, D.M., Bigelow, J.: Similarity: measurement, ordering and betweenness. In: *Knowledge-Based Intelligent Information and Engineering Systems*, pp. 996–1002. Springer (2004)
9. Castelluccio, M., Poggi, G., Sansone, C., Verdoliva, L.: Land use classification in remote sensing images by convolutional neural networks. *arXiv preprint arXiv:1508.00092* (2015)
10. Chatfield, K., Simonyan, K., Vedaldi, A., Zisserman, A.: Return of the devil in the details: Delving deep into convolutional nets. *arXiv preprint arXiv:1405.3531* (2014)
11. Chatzichristofis, S.A., Boutalis, Y.S.: Cedc: color and edge directivity descriptor: a compact descriptor for image indexing and retrieval. In: *Computer Vision Systems*, pp. 312–322. Springer (2008)
12. Cimpoi, M., Maji, S., Kokkinos, I., Mohamed, S., Vedaldi, A.: Describing textures in the wild. In: *Computer Vision and Pattern Recognition (CVPR), 2014 IEEE Conference on*, pp. 3606–3613 (2014)
13. Ciocca, G., Gagliardi, I., Schettini, R.: Quicklook 2: An integrated multimedia system. *Journal of Visual Languages & Computing* **12**(1), 81–103 (2001)
14. Ciocca, G., Schettini, R.: A relevance feedback mechanism for content-based image retrieval. *Information processing & management* **35**(5), 605–632 (1999)
15. Csurka, G., Dance, C., Fan, L., Willamowski, J., Bray, C.: Visual categorization with bags of keypoints. In: *Workshop on statistical learning in computer vision, ECCV*, vol. 1, pp. 1–2. Prague (2004)
16. Cusano, C., Napoletano, P., Schettini, R.: Remote sensing image classification exploiting multiple kernel learning. *IEEE Geoscience and Remote Sensing Letters* **12**(11), 2331–2335 (2015). DOI 10.1109/LGRS.2015.2476365
17. Dai, D., Yang, W.: Satellite image classification via two-layer sparse coding with biased image representation. *Geoscience and Remote Sensing Letters* **8**(1), 173–176 (2011)
18. Datta, R., Joshi, D., Li, J., Wang, J.Z.: Image retrieval: Ideas, influences, and trends of the new age. *ACM Computing Surveys (CSUR)* **40**(2), 5 (2008)
19. Demir, B., Bruzzone, L.: A novel active learning method in relevance feedback for content-based remote sensing image retrieval. *Geoscience and Remote Sensing, IEEE Transactions on* **53**(5), 2323–2334 (2015)
20. Deng, J., Dong, W., Socher, R., Li, L.J., Li, K., Fei-Fei, L.: Imagenet: A large-scale hierarchical image database. In: *IEEE Conference on Computer Vision and Pattern Recognition*, pp. 248–255. IEEE (2009)
21. Deselaers, T., Keysers, D., Ney, H.: Features for image retrieval: an experimental comparison. *Information Retrieval* **11**(2), 77–107 (2008)
22. Ferecatu, M., Boujemaa, N.: Interactive remote-sensing image retrieval using active relevance feedback. *Geoscience and Remote Sensing, IEEE Transactions on* **45**(4), 818–826 (2007)
23. Grauman, K., Leibe, B.: *Visual object recognition*. Morgan & Claypool Publishers (2010)
24. Hanbury, A., Kandaswamy, U., Adjeroh, D.: Illumination-invariant morphological texture classification. In: C. Ronse, L. Najman, E. Decencire (eds.) *Mathematical Morphology: 40 Years On, Computational Imaging and Vision*, vol. 30, pp. 377–386. Springer Netherlands (2005). DOI 10.1007/1-4020-3443-1\_34
25. Haralick, R.: Statistical and structural approaches to texture. *Proc. of the IEEE* **67**(5), 786–804 (1979)





26. Hauta-Kasari, M., Parkkinen, J., Jaaskelainen, T., Lenz, R.: Generalized co-occurrence matrix for multispectral texture analysis. In: *Pattern Recognition, 1996., Proceedings of the 13th International Conference on*, vol. 2, pp. 785–789 vol.2 (1996). DOI 10.1109/ICPR.1996.546930
27. Hong, P., Tian, Q., Huang, T.S.: Incorporate support vector machines to content-based image retrieval with relevance feedback. In: *International Conference on Image Processing*, vol. 3, pp. 750–753. IEEE (2000)
28. Jain, A., Healey, G.: A multiscale representation including opponent color features for texture recognition. *Image Processing, IEEE Transactions on* **7**(1), 124–128 (1998). DOI 10.1109/83.650858
29. Jégou, H., Douze, M., Schmid, C., Pérez, P.: Aggregating local descriptors into a compact image representation. In: *IEEE Conference on Computer Vision and Pattern Recognition (CVPR)*, pp. 3304–3311 (2010)
30. Junior, O.L., Delgado, D., Gonçalves, V., Nunes, U.: Trainable classifier-fusion schemes: an application to pedestrian detection. In: *Intelligent Transportation Systems* (2009)
31. Krizhevsky, A., Sutskever, I., Hinton, G.E.: Imagenet classification with deep convolutional neural networks. In: *Advances in neural information processing systems*, pp. 1097–1105 (2012)
32. Li, J., Allinson, N.M.: Relevance feedback in content-based image retrieval: a survey. In: *Handbook on Neural Information Processing*, pp. 433–469. Springer (2013)
33. Liu, G.H., Yang, J.Y.: Content-based image retrieval using color difference histogram. *Pattern Recognition* **46**(1), 188–198 (2013)
34. Lowe, D.: Distinctive image features from scale-invariant keypoints. *Int'l J. Computer Vision* **60**(2), 91–110 (2004)
35. Mäenpää, T., Pietikäinen, M.: Classification with color and texture: jointly or separately? *Pattern Recognition* **37**(8), 1629–1640 (2004)
36. Manjunath, B.S., Ma, W.Y.: Texture features for browsing and retrieval of image data. *Pattern Analysis and Machine Intelligence, IEEE Transactions on* **18**(8), 837–842 (1996)
37. Manjunath, B.S., Ohm, J.R., Vasudevan, V.V., Yamada, A.: Color and texture descriptors. *Circuits and Systems for Video Technology, IEEE Transactions on* **11**(6), 703–715 (2001)
38. Manning, C.D., Raghavan, P., Schütze, H.: *Introduction to information retrieval*, vol. 1. Cambridge university press Cambridge (2008)
39. Marmanis, D., Datcu, M., Esch, T., Stilla, U.: Deep learning earth observation classification using imagenet pre-trained networks. *IEEE Geoscience and Remote Sensing Letters* **13**(1), 105–109 (2016)
40. Mirmehdi, M., Xie, X., Suri, J.: *Handbook of Texture Analysis*. Imperial College Press (2009)
41. Novak, C.L., Shafer, S., et al.: Anatomy of a color histogram. In: *Computer Vision and Pattern Recognition, 1992. Proceedings CVPR'92., 1992 IEEE Computer Society Conference on*, pp. 599–605. IEEE (1992)
42. Ojala, T., Pietikäinen, M., Mäenpää, T.: Multiresolution gray-scale and rotation invariant texture classification with local binary patterns. *IEEE Trans. Pattern Anal. Mach. Intell.* **24**(7), 971–987 (2002)
43. Oliva, A., Torralba, A.: Modeling the shape of the scene: A holistic representation of the spatial envelope. *Int'l J. Computer Vision* **42**(3), 145–175 (2001)
44. Ozkan, S., Ates, T., Tola, E., Soysal, M., Esen, E.: Performance analysis of state-of-the-art representation methods for geographical image retrieval and categorization. *Geoscience and Remote Sensing Letters, IEEE* **11**(11), 1996–2000 (2014)
45. Pedronette, D.C.G., Calumby, R.T., Torres, R.d.S.: A semi-supervised learning algorithm for relevance feedback and collaborative image retrieval. *EURASIP Journal on Image and Video Processing* **2015**(1), 1–15 (2015)
46. Pietikäinen, M., Nieminen, S., Marszalec, E., Ojala, T.: Accurate color discrimination with classification based on feature distributions. In: *Pattern Recognition, 1996., Proceedings of the 13th International Conference on*, vol. 3, pp. 833–838 vol.3 (1996). DOI 10.1109/ICPR.1996.547285
47. Razavian, A.S., Azizpour, H., Sullivan, J., Carlsson, S.: Cnn features off-the-shelf: an astounding baseline for recognition. In: *Computer Vision and Pattern Recognition Workshops (CVPRW), 2014 IEEE Conference on*, pp. 512–519 (2014)
48. Rui, Y., Huang, T.S.: Relevance feedback techniques in image retrieval. In: *Principles of visual information retrieval*, pp. 219–258. Springer (2001)
49. Rui, Y., Huang, T.S., Chang, S.F.: Image retrieval: Current techniques, promising directions, and open issues. *Journal of visual communication and image representation* **10**(1), 39–62 (1999)
50. Rui, Y., Huang, T.S., Ortega, M., Mehrotra, S.: Relevance feedback: a power tool for interactive content-based image retrieval. *Circuits and Systems for Video Technology, IEEE Transactions on* **8**(5), 644–655 (1998)
51. Schmidhuber, J.: Deep learning in neural networks: An overview. *Neural Networks* **61**, 85–117 (2015)
52. Sermanet, P., Eigen, D., Zhang, X., Mathieu, M., Fergus, R., LeCun, Y.: Overfeat: Integrated recognition, localization and detection using convolutional networks. In: *International Conference on Learning Representations (ICLR 2014)*. CBL (2014)
53. Simonyan, K., Zisserman, A.: Very deep convolutional networks for large-scale image recognition. arXiv preprint arXiv:1409.1556 (2014)
54. Sivic, J., Zisserman, A.: Video google: A text retrieval approach to object matching in videos. In: *Computer Vision, 2003. Proceedings. Ninth IEEE International Conference on*, pp. 1470–1477. IEEE (2003)
55. Smeulders, A.W., Worring, M., Santini, S., Gupta, A., Jain, R.: Content-based image retrieval at the end of the early years. *Pattern Analysis and Machine Intelligence, IEEE Transactions on* **22**(12), 1349–1380 (2000)
56. Thomee, B., Lew, M.S.: Interactive search in image retrieval: a survey. *International Journal of Multimedia Information Retrieval* **1**(2), 71–86 (2012)
57. Tsai, C.F.: Bag-of-words representation in image annotation: A review. *ISRN Artificial Intelligence* **2012** (2012)
58. Vedaldi, A., Lenc, K.: Matconvnet – convolutional neural networks for matlab. CoRR abs/1412.4564 (2014)
59. Veltkamp, R., Burkhardt, H., Kriegel, H.P.: *State-of-the-art in content-based image and video retrieval*, vol. 22. Springer Science & Business Media (2013)
60. Wang, X.Y., Wu, J.F., Yang, H.Y.: Robust image retrieval based on color histogram of local feature regions. *Multimedia Tools and Applications* **49**(2), 323–345 (2010)
61. Xia, G.S., Yang, W., Delon, J., Gousseau, Y., Sun, H., Maître, H., et al.: Structural high-resolution satellite image indexing. In: *ISPRS TC VII Symposium-100 Years ISPRS*, vol. 38, pp. 298–303 (2010)
62. Yang, Y., Newsam, S.: Bag-of-visual-words and spatial extensions for land-use classification. In: *Proc. of the Int'l Conf. on Advances in Geographic Information Systems*, pp. 270–279 (2010)

63. Yang, Y., Newsam, S.: Geographic image retrieval using local invariant features. *Geoscience and Remote Sensing, IEEE Transactions on* **51**(2), 818–832 (2013)
64. Zajić, G., Kojić, N., Radosavljević, V., Rudinac, M., Rudinac, S., Reljin, N., Reljin, I., Reljin, B.: Accelerating of image retrieval in cbr system with relevance feedback. *EURASIP Journal on Advances in Signal Processing* **2007**(1), 1–13 (2007)
65. Zeiler, M.D., Fergus, R.: Visualizing and understanding convolutional networks. In: *Computer Vision—ECCV 2014*, pp. 818–833. Springer (2014)
66. Zhou, X.S., Huang, T.S.: Relevance feedback in image retrieval: A comprehensive review. *Multimedia systems* **8**(6), 536–544 (2003)

categories	image	basic IR	pseudo RF	manual RF	act. learn. RF
agricultural		Vgg M (0.092)	Vgg M (0.066)	Vgg VeryDeep 19 (0.048)	BVLC AlexNet (0.049)
airplane		Vgg VeryDeep 19 (0.247)	Vgg VeryDeep 19 (0.165)	Vgg VeryDeep 19 (0.122)	Vgg S (0.077)
baseballdiamond		BVLC Ref (0.281)	Vgg S (0.187)	Vgg S (0.167)	BVLC Ref (0.076)
beach		Vgg VeryDeep 16 (0.097)	Vgg VeryDeep 16 (0.051)	Vgg VeryDeep 16 (0.049)	Vgg F (0.006)
buildings		Vgg S (0.531)	Vgg M 2048 (0.488)	Vgg M 2048 (0.420)	Vgg M (0.394)
chaparral		BVLC Ref (0.007)	BVLC Ref (0.004)	BVLC Ref (0.004)	BVLC Ref (0.000)
denseresidential		SIFT (0.612)	SIFT (0.577)	SIFT (0.546)	Vgg M 1024 (0.567)
forest		Vgg M (0.040)	Vgg M (0.023)	Vgg M (0.021)	BVLC Ref (0.012)
freeway		Vgg F (0.324)	Vgg F (0.271)	Vgg F (0.265)	Vgg M 2048 (0.220)
golfcourse		Vgg VeryDeep 16 (0.392)	Vgg VeryDeep 19 (0.348)	Vgg VeryDeep 19 (0.319)	Vgg M 2048 (0.265)
harbor		Vgg M 2048 (0.210)	Vgg M 2048 (0.157)	Vgg M 2048 (0.155)	Vgg M 2048 (0.014)
intersection		Vgg M 1024 (0.571)	Vgg M 1024 (0.541)	Vgg M 1024 (0.495)	Vgg M (0.376)
mediumresidential		Vgg M (0.469)	Vgg M (0.444)	Vgg M (0.429)	Vgg M (0.355)
mobilehomepark		Vgg S (0.487)	Vgg S (0.465)	Vgg S (0.437)	Vgg S (0.244)
overpass		Vgg VeryDeep 16 (0.493)	BVLC Ref (0.485)	Vgg VeryDeep 16 (0.439)	Vgg S (0.272)
parkinglot		Vgg F (0.116)	Vgg F (0.075)	Vgg F (0.072)	Vgg F (0.006)
river		Vgg S (0.525)	Vgg S (0.500)	Vgg S (0.455)	Vgg F (0.278)
runway		Vgg S (0.313)	Vgg S (0.282)	Vgg S (0.269)	Vgg S (0.154)
sparseresidential		Vgg VeryDeep 19 (0.393)	Vgg VeryDeep 19 (0.322)	Vgg VeryDeep 19 (0.265)	BVLC AlexNet (0.325)
storagetanks		Vgg VeryDeep 16 (0.582)	Vgg VeryDeep 16 (0.589)	Vgg VeryDeep 16 (0.516)	Vgg M 2048 (0.335)
tenniscourt		Vgg M 2048 (0.557)	Vgg M 2048 (0.532)	Vgg M 2048 (0.447)	Vgg F (0.380)

**Table 9** LandUse dataset: ANMRR evaluation across retrieval schemes and RS image classes . For each class and retrieval scheme is reported the best visual descriptor. Blue color stands for CNN-based descriptors, yellow color stands for local descriptors while cyan color stands for global descriptors.

categories	image	basic IR	pseudo RF	manual RF	act. learn. RF
Airport		BVLC Ref (0.251)	BVLC Ref (0.156)	BVLC Ref (0.133)	Vgg F (0.126)
Beach		BVLC Ref (0.074)	Vgg VeryDeep 16 (0.058)	Vgg M (0.037)	Vgg S (0.059)
Bridge		Vgg VeryDeep 16 (0.347)	Vgg VeryDeep 16 (0.296)	Vgg VeryDeep 16 (0.269)	Vgg VeryDeep 16 (0.174)
Commercial		BVLC Ref (0.330)	BVLC Ref (0.278)	BVLC Ref (0.229)	Dense SIFT (VLAD) (0.264)
Desert		DT-CWT (0.097)	CEDD (0.085)	CEDD (0.072)	Opp. Gabor RGB (0.004)
Farmland		Vgg F (0.337)	Vgg VeryDeep 19 (0.304)	Vgg VeryDeep 19 (0.278)	Vgg M 2048 (0.104)
footballField		Vgg S (0.285)	Vgg S (0.202)	Vgg S (0.133)	Gist RGB (0.052)
Forest		Vgg S (0.132)	BVLC AlexNet (0.074)	BVLC AlexNet (0.069)	Vgg S (0.040)
Industrial		Vgg M (0.361)	Vgg M (0.327)	Vgg M 2048 (0.310)	Spatial Hist. RGB (0.463)
Meadow		Dense SIFT (FV) (0.337)	Dense SIFT (FV) (0.308)	Dense SIFT (FV) (0.291)	Opp. Gabor RGB (0.141)
Mountain		SIFT (0.256)	SIFT (0.196)	SIFT (0.175)	SIFT (0.034)
Park		Dense SIFT (0.345)	Dense SIFT (0.262)	Dense SIFT (0.224)	Dense SIFT (VLAD) (0.252)
Parking		SIFT (0.391)	SIFT (0.367)	SIFT (0.306)	Dense SIFT (VLAD) (0.238)
Pond		DT-CWT (0.490)	DT-CWT (0.487)	DT-CWT (0.425)	Gist RGB (0.218)
Port		BVLC Ref (0.408)	BVLC Ref (0.383)	BVLC Ref (0.363)	Dense SIFT (VLAD) (0.307)
railwayStation		SIFT (0.217)	SIFT (0.183)	SIFT (0.152)	SIFT (0.340)
Residential		Vgg VeryDeep 16 (0.411)	Vgg M 2048 (0.371)	Vgg S (0.334)	Dense SIFT (FV) (0.346)
River		Dense SIFT (FV) (0.522)	Vgg M (0.532)	Vgg M (0.477)	Dense SIFT (VLAD) (0.325)
Viaduct		BVLC Ref (0.280)	BVLC Ref (0.262)	Dense SIFT (FV) (0.242)	Dense SIFT (VLAD) (0.053)

**Table 10** SceneSat dataset: ANMRR evaluation across retrieval schemes and RS image classes . For each class and retrieval scheme is reported the best visual descriptor. Blue color stands for CNN-based descriptors, yellow color stands for local descriptors while cyan color stands for global descriptors.

features	basic IR		pseudo RF		manual RF		act. learn. RF		Overall
	<i>ANMRR</i>	<i>EQC</i>	<i>ANMRR</i>	<i>EQC</i>	<i>ANMRR</i>	<i>EQC</i>	<i>ANMRR</i>	<i>EQC</i>	<i>avg rank</i>
Vgg M 2048	0.410	409	0.367	2045	<b>0.327</b>	2045	0.377	8180	4.76
Vgg M	0.398	819	<b>0.364</b>	4095	0.328	4095	0.389	16380	4.84
Vgg S	0.398	819	0.365	4095	0.328	4095	<b>0.373</b>	16380	4.88
Vgg M 1024	0.422	204	0.378	1020	0.337	1020	0.382	4080	5.04
Vgg F	<b>0.397</b>	819	0.366	4095	0.330	4095	0.400	16380	5.14
Vgg M 128	0.525	25	0.495	125	0.435	125	0.464	500	5.92
BVLC Ref	0.404	819	0.374	4095	0.337	4095	0.411	16380	6.00
DT-CWT	0.628	4	0.632	20	0.599	20	0.635	80	6.26
Vgg VeryDeep 16	0.417	819	0.383	4095	0.345	4095	0.406	16380	6.63
BVLC AlexNet	0.416	819	0.389	4095	0.350	4095	0.405	16380	6.65
Vgg VeryDeep 19	0.427	819	0.394	4095	0.351	4095	0.405	16380	7.12
SIFT	0.597	204	0.609	1020	0.555	1020	0.522	4080	7.28
Dense SIFT	0.637	204	0.640	1020	0.601	1020	0.543	4080	7.42
Dense SIFT (FV)	0.578	8192	0.582	40960	0.535	40960	0.497	163840	7.80
Dense SIFT (VLAD)	0.601	5120	0.603	25600	0.558	25600	0.383	102400	7.91
Opp. Gabor RGB	0.691	52	0.698	260	0.671	260	0.553	1040	8.03
Gabor RGB	0.699	19	0.703	95	0.678	95	0.660	380	8.48
Dense LBP RGB	0.702	204	0.708	1020	0.676	1020	0.630	4080	8.52
DT-CWT L	0.690	1	0.693	5	0.669	5	0.722	20	8.59
LBP RGB	0.708	10	0.712	50	0.682	50	0.730	200	8.89
CEDD	0.710	28	0.718	140	0.687	140	0.696	560	9.04
Hist. H V	0.742	102	0.748	510	0.716	510	0.631	2040	9.54
Gabor L	0.726	6	0.731	30	0.709	30	0.710	120	9.57
LBP L	0.725	48	0.732	240	0.700	240	0.730	960	9.80
Gist RGB	0.744	102	0.766	510	0.714	510	0.606	2040	10.30
HoG	0.737	16	0.745	80	0.711	80	0.690	320	10.55
Hist. <i>rgb</i>	0.751	153	0.760	765	0.729	765	0.649	3060	10.86
Granulometry	0.748	15	0.753	75	0.735	75	0.814	300	10.87
Hist. RGB	0.754	153	0.757	765	0.729	765	0.696	3060	11.61
Hist. L	0.772	51	0.776	255	0.748	255	0.701	1020	11.72
Spatial Hist. RGB	0.764	307	0.783	1535	0.735	1535	0.622	6140	11.92
Coocc. matr.	0.841	1	0.844	5	0.828	5	0.827	20	12.07

**Table 11** Average rank across datasets of each visual descriptor performance. The list of visual descriptors reported in the table is ordered by the average rank (last column of the table) that is obtained by averaging the ranks achieved by each visual descriptor across datasets, retrieval schemes and measures: *ANMRR*, *MAP*, *Pr* at 5,10,50,100 levels, and *EQC*. For sake of completeness, for each retrieval scheme, the table shows the average *ANMRR* across datasets and the *EQC* for each visual descriptor. For each retrieval scheme, the best average *ANMRR* performance is reported in bold.

features	Hist. Inters.	Euclidean	Cosine	Manhattan	$\chi^2$ -square	Length	Time (sec)	<i>EQC</i>
CCH+RIT+FPS <sub>1</sub> +FPS <sub>2</sub> [1]	0.609	0.640	-	0.589	<b>0.575</b>	62	-	12
CCH [1]	0.677	0.726	-	0.677	<b>0.649</b>	20	1.9	4
RIT [1]	<b>0.751</b>	0.769	-	0.751	<b>0.757</b>	20	2.3	4
FPS <sub>1</sub> [1]	0.798	0.731	-	0.740	<b>0.726</b>	14	1.6	2
FPS <sub>2</sub> [1]	0.853	0.805	-	0.790	<b>0.783</b>	8	1.6	1
Texture [63]	-	0.630	-	-	-	-	40.4	-
Local features [63]	-	0.591	-	-	-	-	193.3	-
Dense SIFT (BoVW) [44]	-	-	<b>0.540</b>	-	-	1024	9.4	204
Dense SIFT (VLAD) [44]	-	-	<b>0.460</b>	-	-	25600	129.3	5120
Basic IR with Vgg M	0.429	0.378	0.378	0.386	<b>0.374</b>	4096	-	819
Basic IR with Vgg M 128	0.544	<b>0.488</b>	<b>0.488</b>	0.493	<b>0.488</b>	128	-	25
Pseudo RF Vgg M	0.423	<b>0.344</b>	<b>0.344</b>	0.363	<b>0.344</b>	4096	-	4095
Pseudo RF Vgg M 128	0.550	0.470	0.470	0.466	<b>0.458</b>	128	-	125
Manual RF Vgg M	0.392	0.316	0.316	0.333	<b>0.315</b>	4096	-	4095
Manual RF Vgg M 128	0.497	0.422	0.422	0.416	<b>0.410</b>	128	-	125
Active Learning RF Vgg M	<b>0.247</b>	-	-	-	-	4096	-	16380
Active Learning RF Vgg M 128	<b>0.333</b>	-	-	-	-	128	-	500

**Table 12** *ANMRR* comparison on the LandUse dataset. The lower is the result, the better is the performance. For each row the best result is reported in bold.